Building and Environment 95 (2016) 160–170

Contents lists available at ScienceDirect

Building and Environment

journal homepage: www.elsevier.com/locate/buildenv

Development of an urban canopy model for the evaluation of urban thermal climate with snow cover in severe cold regions

Taotao Shui [a], Jing Liu [a, b, *], Pengcheng Zhang [a], Shengjun Liu [c], Zhiqing Zhao [c]

[a] School of Municipal and Environmental Engineering, Harbin Institute of Technology, Harbin 150090, China
[b] State Key Laboratory of Urban Water Resource and Environment, Harbin Institute of Technology, Harbin 150090, China
[c] Urban Planning & Design Institute, Harbin Institute of Technology, Harbin 150006, China

ARTICLE INFO

Article history:
Received 14 May 2015
Received in revised form
10 September 2015
Accepted 11 September 2015
Available online 14 September 2015

Keywords:
Urban canopy model
Snow cover
Thermal climate
Numerical modeling

ABSTRACT

Snow plays an important role in determining heat and moisture exchanges between the underlying surface and atmosphere in winter. However, the effect of snow cover is not considered or assumed to be negligible in existing urban canopy energy balance models. In this paper, a one-dimensional snow model that accounts for heat transfer within snow cover is developed, and the model is implemented into an urban canopy energy balance model to simulate energy and moisture exchanges in cold urban areas with stable snow cover. The numerical methods of the snow model and the urban canopy model are demonstrated first, and the urban canopy model is subsequently used to simulate the thermal climate of a residential area dynamically in Yichun, China during winter. The results indicate that the existence of snow cover decreases the outdoor air temperature by 0.15 °C on average and 1.16 °C at maximum. In addition, the outdoor mean SET* increases 0.43 °C with the removal of snow cover, indicating that the thermal comfort of people outside decreases due to the presence of snow cover.

1. Introduction

With rapid economic growth, there is a growing number of population shifts from rural to urban areas. In the past several decades, the urbanization process has undergone a notable development in China, with the level of urbanization increasing from 17.9% in 1978 to 51.27% in 2011, representing an average annual growth rate of 1.02% [1]. Many studies have shown that the process of urbanization has negative impacts on energy consumption, local thermal conditions, and air quality in urban areas [2–6]. The incidence of and concern about Urban Heat Island (UHI) and haze phenomena have increased in recent years. To create a better urban microclimate, it is necessary to analyze how urban morphology and underlying surface schemes influence the urban microclimate.

Many studies have been conducted to investigate the urban thermal climate; for example, the formation of UHI has been reported in different climatic regions worldwide, e.g., Padua [7], Columbus [8], Delhi [9], Beijing [10], London [11], Moscow [12]. These studies show that the urban thermal climate is strongly influenced by local meteorological conditions, land cover pattern and resident activities. In contrast to the situation in summer, during the winter in cold regions, solar radiation decreases dramatically, and the albedo of the ground changes due to the snow covering the urban underlying surface. In addition, the UHI mitigation strategies that are beneficial in summer may have a detrimental effect in winter. For example, cool roof technologies have been proved as effective strategies to mitigate UHI and optimize indoor thermal performance in summer, while the increasing of roof's albedo also brings slight winter penalties [13–18]. Besides, McPherson stated that high-branching shade trees can promote both shade and wind in summer, while in winter, the shading effect reduces solar radiation access to walls; thus, evergreen trees are not suitable for green roofs in cold climates [19]. Therefore, urban thermal climate and climatic-responsive strategies in winter are quite different from those in summer. To date, studies on the urban thermal climate of severe cold regions in winter are still scarce. Although there has been some research on UHI [9,12,20], thermal comfort [21–23] and energy conservation [24,25] in winter, these studies have mainly based on field experiment data. Due to the limitations of field measurement, experimental conditions, such as meteorological data and land patterns, are uncontrollable during the measurement period, and detailed information is difficult to obtain. In addition,

* Corresponding author. School of Municipal and Environmental Engineering, Harbin Institute of Technology, Harbin 150090, China.
E-mail address: liujinghit0@163.com (J. Liu).

http://dx.doi.org/10.1016/j.buildenv.2015.09.016
0360-1323/

the majority of study objects of these studies are single or several buildings rather than an urban area.

In winter, snow plays an important role in determining heat and moisture exchanges between the land surface and the atmosphere. Walsh et al. [26] found that snow cover accounts for approximately 10%–20% of the variation in monthly temperature throughout the United States. Mote's [27] work demonstrated that snow cover can result in daily temperature decreases throughout central North America. Compared to low-latitude cities, the urban thermal climate of cities in severe cold regions have different properties in winter due to the presence of stable snow cover and unique characteristics of climatic features, urban morphology and underlying surface schemes. Existing studies of snow in urban areas are mainly focused on two aspects: 1) predicting the development of wind-driven snowdrift and partial snow distribution around buildings using computational fluid dynamics (CFD) methods [28–32]; 2) examining the surface energy budget during the snow-cover period by continuous measurements using the eddy covariance technique, which are mostly conducted in Montreal, Canada [33–35]. In addition, using the Montreal Urban Snow Experiment 2005 database, Lemonsu et al. [36,37] examined the ability of the Town Energy Balance (TEB, [38]) canopy model's performance under snowy conditions. With the exception of the TEB model, the effect of snow cover on urban thermal climates is rarely taken into account in urban canopy models. Grimmond et al. [39,40] evaluated and compared the methods and performance of a broad range of urban energy balance models, and the effect of snow cover is not considered or assumed as negligible in these models, indicating that these urban energy balance models are not suitable for the study of urban thermal climate in severe cold regions with snow cover.

In this paper, a one-dimensional snow model that accounts for heat transfer within snow cover is developed, and the model is implemented into an urban canopy energy balance model (called UDC) to simulate energy and moisture exchanges in cold urban areas with stable snow cover. Field measurements were collected to validate the snow model. In addition, the thermal climate of a residential area in Yichun, China, was dynamically simulated and evaluated using the revised UDC model. The objective here is to investigate the impact of snow cover on the local thermal climate. The results show that the existence of snow cover leads to a depression of the outdoor air temperature. Furthermore, the thermal comfort for people outside has deteriorated due to the presence of snow cover.

2. Model development and validation of heat exchange in snow

Heat exchange in snow is simulated using a one-dimensional snow model that is based on energy balance. The snow model is designed to calculate the temperature within the snow cover and the energy exchange between the snow cover, soil and atmosphere. The framework of the model is briefly introduced below. Field measurements were carried out to validate the accuracy of the snow model, which are explained in more detail in Section 4.

2.1. The constitution of snow cover

Wei et al. [41] reported that there are two types of snow cover in China: dry-cold snow cover and humid-warm snow cover. In northeast China, under continental climatic conditions, the winter is long, dry and severely cold. The snow cover in northeast China shows characteristics of dry-cold snow cover: low water content, small density, large temperature gradient, etc. In this study, the snow cover is considered dry-cold and stable with no snow melt during the study period, meaning that the snow is mostly composed of ice and air and that the volumetric water content can be regarded as 0. Thus, the snow volume V_s (m^3/m^2) is composed of two parts: ice volume V_i (m^3/m^2) and air volume V_a (m^3/m^2):

$$V_s = V_i + V_a \tag{1}$$

The volumetric fraction of ice, θ_i, and the volumetric fraction of air, θ_a, can be calculated as

$$\theta_i = \frac{V_i}{V_s}, \theta_a = \frac{V_a}{V_s} \tag{2}$$

By definition, the volumetric fraction is between 0 and 1, and the following relationship should be rigidly enforced

$$\theta_i + \theta_a = 1 \tag{3}$$

Compared to the ice density ρ_i (kg/m^3), the air density can be neglected. Therefore, the density of snow cover, ρ_s (kg/m^3), can be expressed by

$$\rho_s = \rho_i \theta_i \tag{4}$$

2.2. Numerical method of the snow model

The heat exchanges between the snow cover, soil and atmosphere, including radiation, heat transfer and sublimation, are considered. A schematic diagram of heat transfer within the snow cover and soil in the snow model is shown in Fig. 1.

Snow cover is divided into several layers along the vertical direction. The temperature of the snow layer is represented by the intermediate snow temperature of each layer, while the density of every layer is uniform. The heat balance equations of the snow model are calculated as follows:

Top layer:

$$\frac{\partial}{\partial t}\{c_{v,s,l}\Delta Z_s T_{s,l}\} = C_{s,l+1} + R_{ns,l} + R_{nl} + H_s - lE_s \tag{5}$$

Inner layers:

$$\frac{\partial}{\partial t}\{c_{vs,l}\Delta Z_s T_{s,l}\} = -C_{s,l-1} + C_{s,l+1} + R_{ns,l} \tag{6}$$

Bottom layer:

$$\frac{\partial}{\partial t}\{c_{vs,l}\Delta Z_s T_{s,l}\} = -C_{s,l-1} + C_{sx} + R_{ns,l} \tag{7}$$

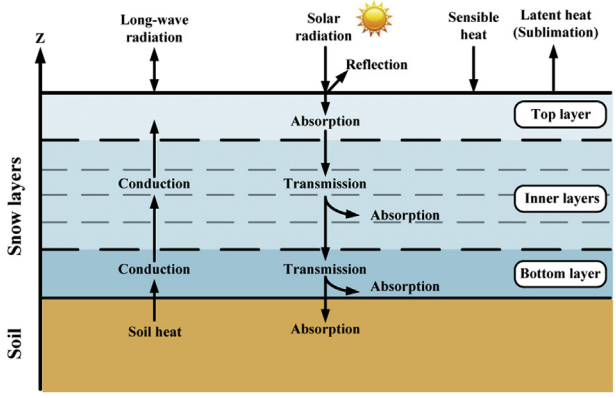

Fig. 1. Schematic diagram of heat transfer in the snow model.

where $c_{vs,\ l}$ is the volume heat capacity of each snow layer (J/(m^3·K)); ΔZ_s is the thickness of each snow layer (m); $T_{s,\ l}$ is the temperature of each snow layer (K); $C_{s,\ l\text{-}1}$ and $C_{s,\ l+1}$ are the conduction heat fluxes caused by the upper and lower snow layer temperature differences (W/m^2), respectively; C_{sx} is the conduction heat flux at the contact surface of snow and soil (W/m^2); $R_{ns,\ l}$ is the solar radiation that is absorbed by each snow layer (W/m^2); R_{nl} is the net long-wave radiation heat flux (W/m^2); H_s is the sensible heat flux (W/m^2); and lE_s is the latent heat of sublimation (W/m^2).

The volume heat capacity of snow, c_{vs}, can be calculated as follows:

$$c_{vs} = \theta_i \cdot c_{vi} \tag{8}$$

where the volume heat capacity of ice (J/(m^3·K)), c_{vi}, is given by Ref. [42].

$$c_{vi} = 92.96 + 7.73 \cdot T_s \tag{9}$$

The conduction heat flux, $C_{s,\ l\text{-}1}$, $C_{s,\ l+1}$, is given by

$$C_{s,l-1} = -\lambda_s \frac{T_{s,l} - T_{s,l-1}}{\Delta Z_s} \tag{10}$$

$$C_{s,l+1} = -\lambda_s \frac{T_{s,l+1} - T_{s,l}}{\Delta Z_s} \tag{11}$$

where λ_s is the thermal conductivity of snow (W/(K·m)), and $T_{s,\ l-1}$ and $T_{s,\ l+1}$ are the temperatures of the upper and lower snow layers (K), respectively.

The thermal conductivity of snow, λ_s, is sensitively related to the snow density, ρ_s [43]

$$\lambda_s = s_k \rho_s^2 \tag{12}$$

where s_k is an empirical coefficient.

In this model, C_{sx} is computed as follows:

$$C_{sx} = \frac{1}{\frac{\Delta Z_s/2}{\lambda_s} + \frac{\Delta Z_{cx}/2}{\lambda_x} + R_c} (T_{cx} - T_s) \tag{13}$$

where ΔZ_{cx} is the thickness of the soil surface layer (m); λ_x is the thermal conductivity of frozen soil (W/(K·m)); T_{cx} is the temperature of the soil surface layer (K); and R_c is the thermal contact resistance of snow and soil (K·m^2/W). R_c is given by Ref. [44].

$$R_c = 0.6 \times 10^{-3} \exp(5.3\theta_a) \tag{14}$$

Due to the translucency of snow, solar radiation will be constantly absorbed by snow in the process of passing down, resulting in an increased temperature of snow. The attenuation rate of solar radiant energy in snow follows the Beer–Lambert law. Thus, $R_{ns,\ l}$ can be calculated as.

Top layer:

$$R_{ns,l} = R_s\downarrow (1 - \alpha_s)\left(1 - e^{-\mu \Delta Z_s}\right) \tag{15}$$

Inner layers:

$$R_{ns,l} = R_{ns,l-1}\left(e^{-\mu Z_s} - e^{-\mu\left(Z_{s,l} + \Delta Z_s\right)}\right) \tag{16}$$

where $R_s\downarrow$ is the downward solar radiation flux (W/m^2); α_s is the snow surface albedo; μ is the absorption coefficient; and $Z_{s,\ l}$ is the depth of the current snow layer (m).

The net long-wave radiation heat flux, R_{nl}, is given by

$$R_{nl} = R_l\downarrow - \varepsilon_s \sigma (T_{ss} + 273.15)^4 \tag{17}$$

where $R_l\downarrow$ is the downward long-wave radiation flux (W/m^2); ε_s is the snow surface emission rate, chosen as 0.82 [45]; σ is the Stephan–Boltzmann constant, 5.67×10^{-8} W/(m^2·K^4); and T_{ss} is the temperature of the surface snow layer.

The sensible heat flux, H_s, and the latent heat, lE_s, are given by the bulk heat transfer method:

$$H_s = \rho_a c_p C_h U_{1.0} (T_{1.0} - T_{ss}) \tag{18}$$

$$lE_s = \rho_a \lambda_s C_e U_{1.0} (X_{1.0} - X_{ss}) \tag{19}$$

where $U_{1.0}$, $T_{1.0}$, and $X_{1.0}$ are the wind velocity (m/s), temperature (K) and specific humidity (g/kg) at 1.0 m aboveground, respectively; ρ_a is the air density (kg/m^3); c_p is the specific heat of air (kJ/(kg·K)); C_h is the bulk transfer coefficient for sensible heat; λ_s is the snow latent heat of sublimation (kJ/kg); C_e is the bulk transfer coefficient for water vapor; and X_{ss} is the saturated specific humidity of the snow surface (g/kg). The bulk transfer coefficients over the snow surface were determined experimentally by Kondo and Yamazawa with $C_h = 2.0 \times 10^{-3}$ and $C_e = 2.1 \times 10^{-3}$ for a reference height of 1 m [46].

3. UDC modeling

UDC is an urban canopy energy balance model that is adapted for the dynamic study of the urban thermal climate and local heat island intensity change. The UDC model includes the following sub-models: urban layout sub-model, local climate sub-model, building heat and moisture load sub-model, urban underlying surface heat and mass transfer sub-model, solar radiation sub-model and thermal comfort sub-model. These sub-models are dynamically coupled. The numerical methods of the sub-models that are related to this study are briefly presented below. Further detailed information and validation of this model can be found in Refs. [47–49]. The one-dimensional snow model that is developed in this study is implemented into UDC as a sub-model. The framework diagram of the revised UDC model is presented in Fig. 2.

3.1. Urban layout sub-model

To simplify the calculation, the real urban configuration is converted into a hypothetical urban area. After statistical analysis of the urban architectural layout, all buildings are modeled to be rectangular, and roads are divided into three sections with 27 grid cells according to their orientation, as seen in Fig. 3.

The floor area ratio φ is given by

$$\varphi = \frac{L_{BX} L_{BY}}{L_{SX} L_{SY}} \times N \tag{20}$$

where L_{BX} and L_{BY} are the lengths of the building in the X and Y directions (m), respectively; L_{SX} and L_{SY} are the lengths of the building and its adjacent street in the X and Y directions (m), respectively; and N is the average height of the buildings in the urban canopy (m).

3.2. Local climate sub-model

The model that is utilized in this study, which can compute the temporal vertical distribution of temperature, wind velocity and specific humidity in the boundary layer, refers to Kondo and Liu's one-dimensional canopy model [50], and appropriate modification was made in our model.

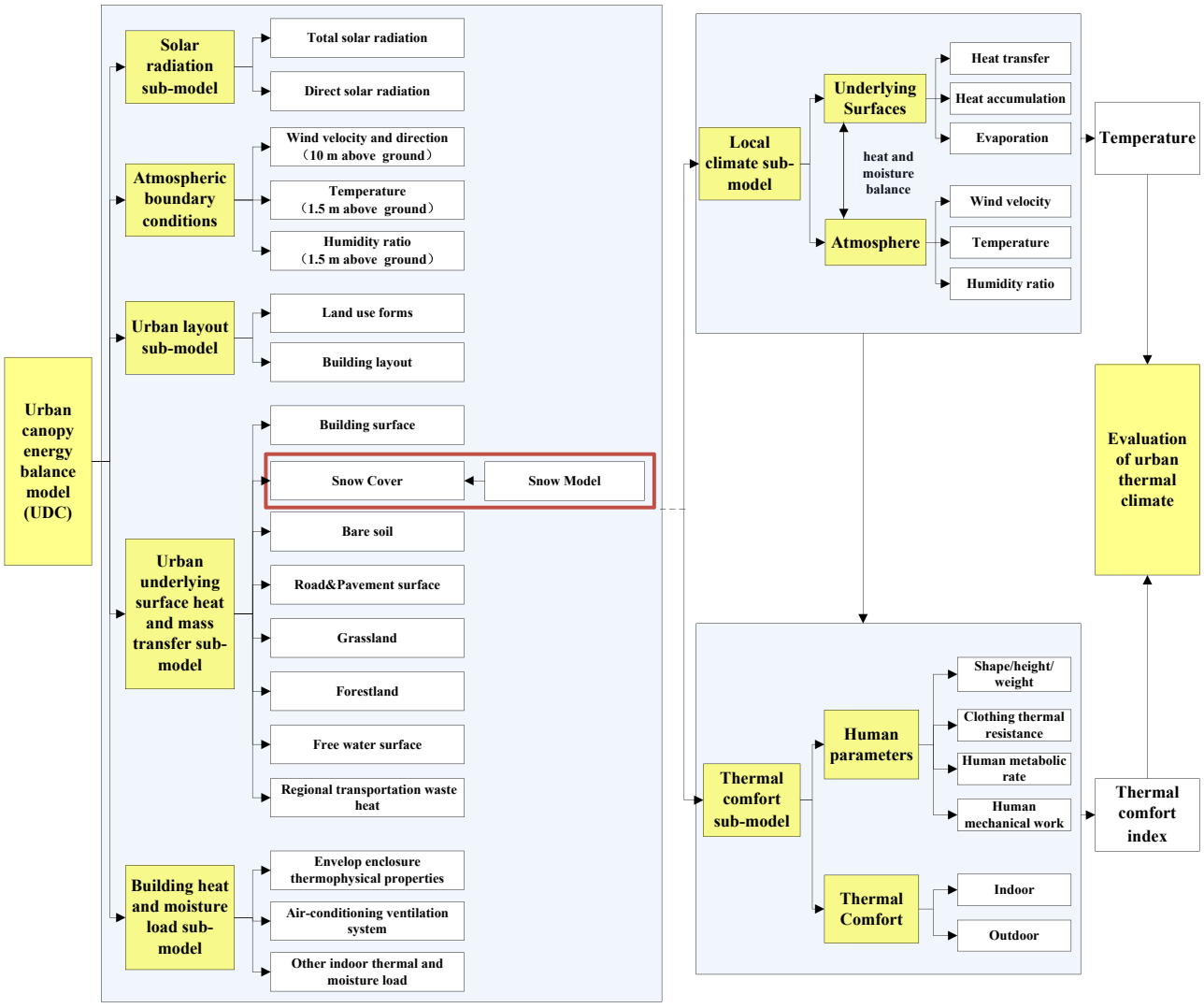

Fig. 2. Framework diagram in UDC modeling.

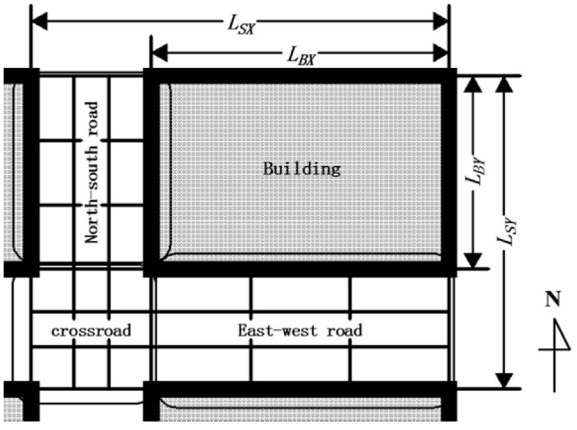

Fig. 3. Schematic of the hypothetical urban district and meshes for outdoor calculation.

The governing equations of momentum, heat and moisture are modeled by

$$\frac{\partial U(z,t)}{\partial t} = \frac{1}{m}\frac{\partial}{\partial z}\left(-m\langle u'w'\rangle\right) - caU|U| \tag{21}$$

$$\rho_a c_p V \frac{\partial \Theta(z,t)}{\partial t} = \rho_a c_p V \frac{1}{m}\frac{\partial}{\partial z}\left(-m\langle \theta'w'\rangle\right) + G \tag{22}$$

$$\rho_a V \frac{\partial X(z,t)}{\partial t} = \rho_a V \frac{1}{m}\frac{\partial}{\partial z}\left(-m\langle x'w'\rangle\right) + S \tag{23}$$

where $U(z, t)$ is the outdoor wind velocity (m/s); m is the ratio of the volume density of the fluid; -<$u'w'$> is the Reynolds stress (m^2/s^2); c is the resistance coefficient; a is the fraction of the building surface area density (m^{-1}); V is the volume of air in the urban canopy (m^3); $\Theta(z, t)$ is the outdoor temperature (K); -<$\theta'w'$> is the kinematical turbulence buoyancy flux (m·K/s); G is the sensible heat source (W); $X(z, t)$ is the outdoor specific humidity (g/kg); -<$x'w'$> is the kinematical turbulence moisture flux (m·g/(kg·s)); and S is the moisture source (kg/s).

It should be noted that the attenuation effect of trees on the wind should be taken into account when trees exist in the study area. Thus, the additional term $-c_t a_t U|U|$ should be added to the

right side of Eq. (21), where c_t is the drag coefficient of trees, and a_t is the leaf area density of the tree crown (m^2/m^3).

3.3. Urban underlying surface heat and mass transfer sub-model

The urban underlying surface as considered in this model includes the following common forms: impervious artificial surface (such as building surface, concrete road, etc.), bare soil, grass, forestland and free water surface. However, snow cover in winter was not considered prior to this study.

The heat balance equation of underlying surface is defined as

$$R_{n,i} = R_s\downarrow - \varepsilon_i\sigma T_i^4 + \varepsilon_i\left(F_{is}\underset{i\neq j}{R_l} + \sum_j F_{ij}\varepsilon_j\sigma T_j^4\right)_s = H_i + lE_i + CD_i \tag{24}$$

where $R_{n;i}$ is the net radiation of a wall or earth facet i (W/m^2); ε is the surface emissivity; T is the absolute temperature (K); F is the view factor between two facets; H is the upward sensible heat flux of the underlying surface (W/m^2); lE is the upward latent heat flux of the underlying surface (W/m^2); and CD is the internal heat flux of the underlying surface (W/m^2).

The calculation of the sensible heat flux H_a and moisture flux EV_a of impervious artificial surface [51,52], bare soil surface [53] and grass surface [54] can be found elsewhere.

3.4. Solar radiation sub-model

The calculation of the radiation flux within the urban canopy is extremely complicated due to the existence of buildings. In this study, the photon-tracking method is adopted to calculate the viewing factor [55].

In addition, when trees exist in the study area, the attenuation effect of trees on solar radiation is considered in this model. In this study, it is assumed that the attenuation effect is independent of the radiation wavelength and incident angle. Thus, the attenuation effect is only affected by the distance of light through the canopy. In addition, the complex refraction and reflection effect between leaves within the canopy is also ignored. Therefore, the attenuation rate η_t is defined as

$$\eta_t = 1 - \exp(-k'al) \tag{25}$$

where k' is the coefficient related to attenuation, and l is the distance of light through the canopy (m).

3.5. Thermal comfort sub-model

Until now, much work has been carried out to study indoor thermal comfort, and a number of thermal climatic indices have been proposed for indoor thermal comfort assessments. However, thermal comfort in the outdoor environment has received little research to date. Most of the existing thermal indices are based on steady-state energy-balance models of the human body, and their use is restricted to environments in which people remain for a long time [56]. The standard effective temperature (SET*) was developed based on a dynamic two-node model (2NM) of human temperature regulation [57]. Different from other comfort models according to subjective perception, SET* is established based on a human thermophysiological model and calculated through energy balance between the human body and ambient atmosphere. Although expressed as temperature, SET* actually reflects the thermal sensation in a specific environment. Therefore, SET* is suitable for different outdoor conditions. Compared to several other thermal comfort indices in evaluating outdoor and semi-outdoor thermal comfort, SET* is better for assessing the thermal sensation of outdoor subjects because it successfully relates environmental variables with a person's thermal sense [58,59]. Kinouchi [60] and Honjo [61] also reported that SET* is appropriate for use in the outdoor environment. Therefore, SET* was chosen to evaluate outdoor thermal comfort in this study.

In our model, the method used to calculate SET* referred to Gagge [57]. SET* is defined mathematically as follows:

$$Q_{sk} = \alpha'_{SET}(T_{sk} - SET^*) + \omega\alpha'_{eSET}(P_{sk} - 0.5P_{SET}) \tag{26}$$

where Q_{sk} is the total heat loss from the skin (W/m^2); α'_{SET} is the sensible heat transfer coefficient including clothing ($W/m^2\cdot K$)); T_{sk} is the skin temperature (°C); ω is the skin wettedness; α'_{eSET} is the evaporative heat transfer coefficient including clothing ($W/(m^2\cdot kPa)$); P_{sk} is the water vapor pressure (kPa); and P_{SET} is the saturated water vapor pressure at T_{sk} (kPa).

The mean radiant temperature (MRT) is a key variable in making thermal calculations for the human body; however, it is one of the most difficult parameters to determine. Detailed description of the calculation method of indoor and outdoor MRT that is adopted in the UDC model can be found in Zhu [47].

4. Field measurement and model validation of snow cover

4.1. Study area and instruments

To validate the accuracy of the snow model, field measurements were carried out in a certain campus in Harbin (45°45′N, 126°40′E). Harbin is located in the severely cold region of northeast China, as shown in Fig. 4, and there is always a steady layer of snow cover in winter. The campus is open, and the snow cover has not been cleaned. The measured snow temperature was compared to the simulated results.

The meteorological data were obtained from the JY2TRM-ZS2 automatic weather station, and the snow temperature was measured using the BES-02 temperature and moisture acquisition recorder. The main measured parameters and technique data for the instruments are summarized in Table 1.

Fig. 4. Climatic regions of China and the site of Harbin.

4.2. Snow model validation

Measurements were collected on open land with 18.5 cm of snow cover in the natural state with no cleaning or crushing by vehicles. Three BES-02 temperature sensors were placed on the top layer, inner layer and bottom layer of snow, as shown in Fig. 5. The measurement period was from 11:00 am, December 30, 2013, to 10:15 am, December 31, 2013. The interval for the temperature data acquisition time was 1 min.

A comparison between the measured and simulated snow temperature is shown in Fig. 6. It can be observed from the figure that the simulated and measured snow temperatures in the top layer have similar patterns. Furthermore, there are discrepancies and a slight delay between the calculated and measured results. The discrepancies and delay are due to the deviation in the physical parameters (e.g. heat capacity, albedo, and thermal conductivity) of snow and soil between the actual values and the values that were chosen in the model, which will affect the accuracy of the simulation. Besides, the bulk transfer coefficients used in our model are experimental values based on Kondo and Yamazawa's study [46], which may differ from the real situation in our case. For the inner and bottom layers, unlike the measured data, the calculated temperature is relatively stable over time. This is because the volumetric fraction of air, θ_a, is considered constant in the snow model. In the snow model, the air in the snow layer, which has no interaction with the ambient atmosphere, can only affect the snow's density and thermal capacity. However, actual snow is fluffy. Due to the infiltration of cold air, the ambient air has a significantly influence on the inner layer's temperature. Thus, the measured values fluctuate more significantly than do the calculated values.

Average and mean error (ME) of simulated and measured snow temperature at different depths are summarized in Table 2. ME is defined as follows:

$$ME = \frac{\sum (S_i - M_i)}{n} \quad (27)$$

where S_i is the simulated value; M_i is the measured value; and n is the number of samples.

As shown in Table 2, ME is −0.08 °C for the top layer, −0.25 °C for the inner layer, and −0.06 °C for the bottom layer, respectively, which indicates the snow model captured the average snow temperature at different depths with adequate accuracy. Although discrepancies exist in detail between simulated and measured snow temperature, the variation trends of snow temperature are well reproduced. Since our snow model is a simple one-dimensional model, the aim of developing this model is to grasp the variation trend of snow temperature and reflect the average effect of snow on local climate. Thus the model is precise enough in this study.

5. Effect of the snow cover on the local thermal climate and thermal comfort

In this study, the thermal climate of a residential area in winter was investigated using the revised UDC model. Simulations were carried out for the residential area with or without snow covering underlying surfaces to evaluate the impact of snow cover on the local thermal climate. The outdoor air temperature, underlying surface temperature, building exterior wall temperature and outdoor thermal comfort were analyzed.

Table 1
Main measured parameters and technique data for the instruments.

Parameters	Resolution	Precision/Range
Wind velocity	0.1 m/s	±0.3 m/s (0 ~ 70 m/s)
Wind direction	3°	±3° (0 ~ 360°)
Air temperature	0.1 °C	±0.2 °C (−50 ~ 150 °C)
Radiation flux	1 W/m^2	±5% (0 ~ 2000 W/m^2)
Snow temperature	0.1 °C	±0.2 °C (−50 ~ 120 °C)

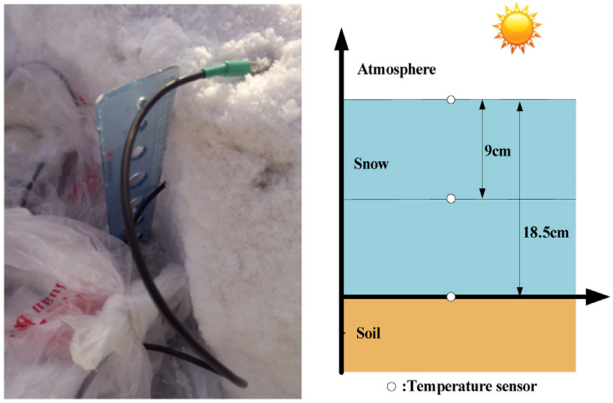

Fig. 5. A sketch of the field measurements.

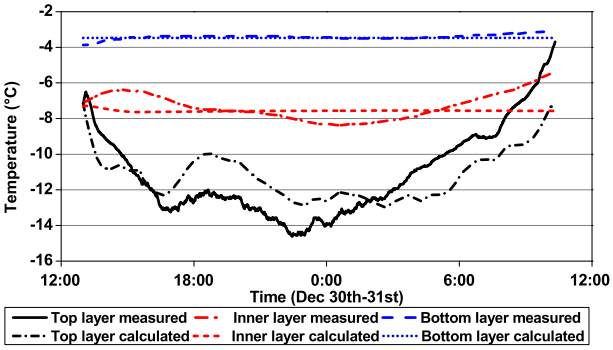

Fig. 6. Comparison of the calculated and measured results for snow temperature.

Table 2
Size and structures of the residential building.

	Average (°C)		ME (°C)
	Simulated	Measured	
Top layer	−11.21	−11.13	−0.08
Inner layer	−7.56	−7.31	−0.25
Bottom layer	−3.48	−3.41	−0.06

5.1. Study area

The study site is a residential area in Yichun (47°85′N, 128°84′E). Yichun is a large city in the northernmost region of China. The location of Yichun and the residential area to be studied is shown in Fig. 7. All of the buildings in the residential area are slab-type with the same specification. In this study, these buildings were simplified to identical cuboids with a bottom area of 676 m^2. The size and structures of typical residential building are summarized in Table 3. The parameters of the building's envelop thermal performance are determined according to [62]. Except for building coverage, the underlying surface is made up of asphalt pavement and soil, whose area is 1:1.5.

To investigate the effect of snow cover on the local thermal comfort, simulations were conducted when the underlying surface

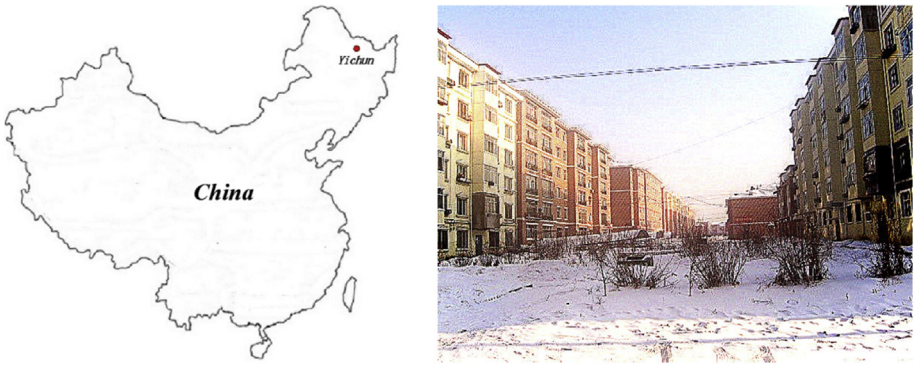

Fig. 7. The location of Yichun in China and the residential area to be studied.

Table 3
Size and structures of the residential building.

Parameters	Value
Length × width	26 m × 26 m
Floor height	3 m
Canopy height/No. of story	18 m/6
Floor area ratio	1.345
Exterior wall	solid clay brick (240 mm) & expanded polystyrene board (120 mm) with K = 0.35 W/(m^2·K)
Exterior window	6 + 12+6 mm Low-E glass with K = 1.8 W/(m^2·K)
Ratio of glazing	40%
Design indoor temperature for heating	18 °C

was covered by a 20 cm snow layer (Case 1), and the results were then compared with the situation in which there is no snow cover (Case 2).

5.2. Meteorological conditions

In this study, the meteorological data was chosen from the typical meteorological year (TMY) of Yichun based on a typical meteorological database [63]. The TMY consists of 12 typical meteorological months (TMM) that are selected from the observations. The method to select TMMs in the typical meteorological database can be found in Zhang [64]. According to the TMM data, December is the coldest month of Yichun in winter. Therefore, the hourly data from December 1 to December 31 was used as input data, as shown in Fig. 8. It can be observed from Fig. 8 that the outdoor temperature is very low, no precipitation occurred during the computing period, and there was a large temperature difference between daytime and nighttime. The highest temperature was −5.69 °C, and the lowest temperature was −28.69 °C, with an average temperature of approximately −16.78 °C. The air was dry, and the specific humidity mainly fluctuated from 0.3 to 1.0 g/kg. The daily solar radiation intensity was comparatively small, with a maximum value of less than 420 W/m^2. The site is windy, and the wind velocity changes within a large range from 0.69 m/s to 13.8 m/s with an average velocity of 3.88 m/s. The most frequent wind directions were south-west and west-south west.

To eliminate the influence of the initial conditions and the hysteresis effect of calculation, the data of first three days were used for the preliminary calculation, while the calculation results of the last four weeks were adopted for analysis in this paper.

5.3. Underlying surface temperature

Fig. 9 shows the comparison of the underlying surface temperature of Case 1 and Case 2. It should be noted that the underlying surface temperature of Case 2 is the mean surface temperature of asphalt pavement and soil. The surface temperature difference, $T_{s,\ diff}$, is defined as.

$$T_{s,diff} = T_{s,s} - T_{s,ns} \tag{28}$$

where $T_{s,\ s}$ is the snow surface temperature when snow cover is considered, and $T_{s,\ ns}$ is the underlying surface temperature with no snow cover.

As seen in Fig. 9, the surface temperature of snow cover is much less than the underlying surface temperature with no snow cover. Specifically, the average surface temperature of snow cover in Case 1 is −15.58 °C, and the average surface temperature of soil and asphalt pavement in Case 2 is −12.39 °C. The surface temperature increases 3.19 °C more with snow cover removed, and the maximum difference can reach 10.89 °C. Compared to asphalt pavement and soil, due to the higher albedo and transmittance of snow, more solar radiation is reflected and less radiation is absorbed by the snow cover, leading to the significant temperature depression of snow surface in Case 1.

5.4. Building exterior wall temperature

Fig. 10 shows the comparison of the building exterior wall temperature between Case 1 and Case 2. It should be noted that the building exterior wall temperature is the average temperature of the building exterior walls for each orientation. The exterior wall temperature difference, $R_{ref,\ diff}$, is defined as.

$$T_{wall,diff} = T_{wall,s} - T_{wall,ns} \tag{29}$$

where $T_{wall,\ s}$ is the exterior wall temperature in the presence of snow cover, and $T_{wall,\ ns}$ is the exterior wall temperature when there is no snow cover.

It can be observed from the figure that the building exterior wall temperature is higher, mostly during the daytime, with the presence of snow cover: the average exterior wall temperature

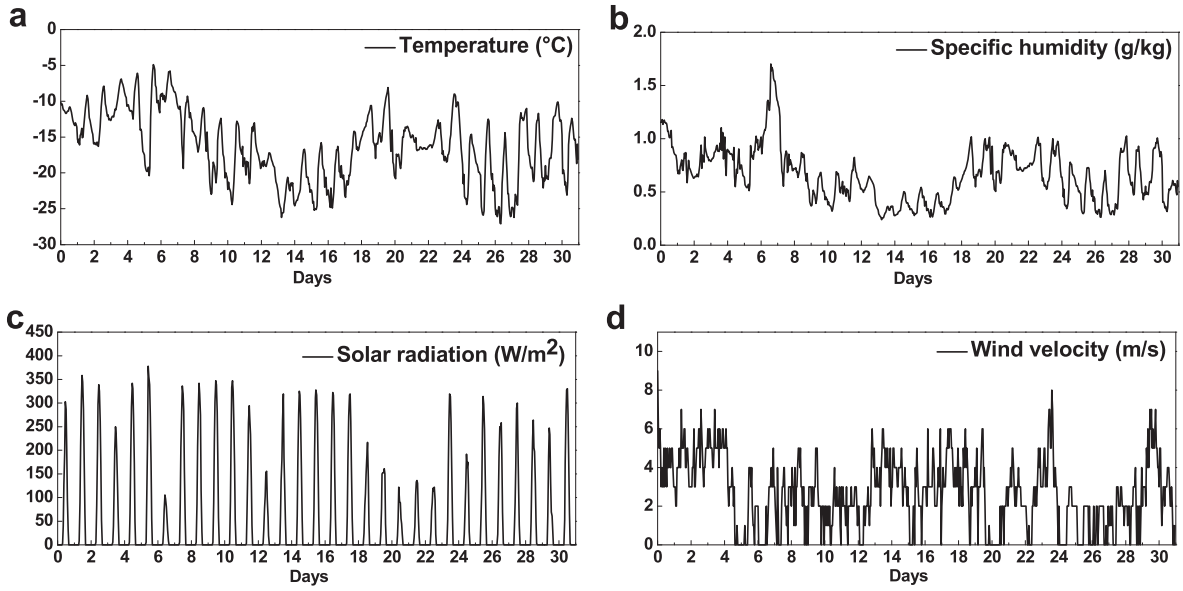

Fig. 8. Hourly meteorological parameters as measured during the calculation period.

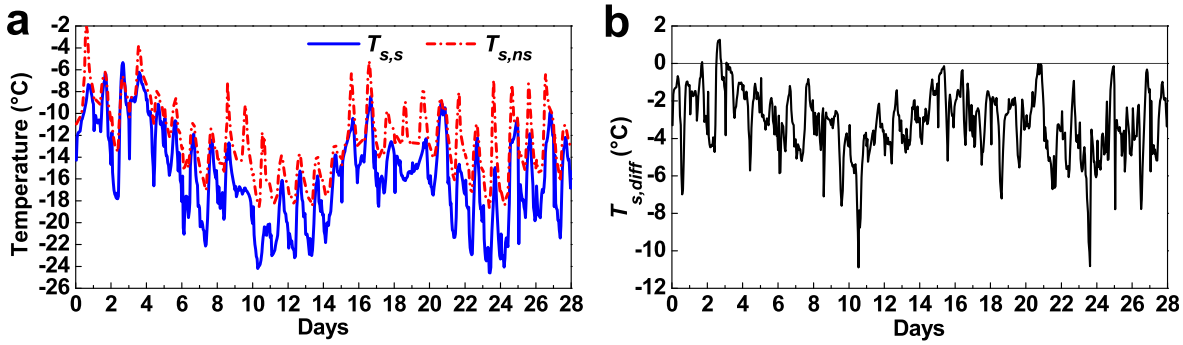

Fig. 9. Comparison of the underlying surface temperature (°C) of Case 1 and Case 2: (a) underlying surface temperature, $T_{s,\ s}$ and $T_{s,\ ns}$; (b) underlying surface temperature difference, $T_{s,\ diff}$.

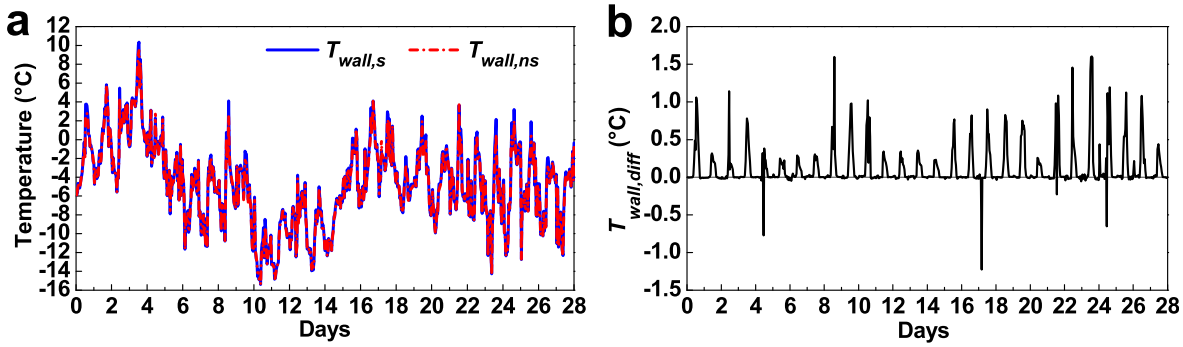

Fig. 10. Comparison of the building exterior wall temperature (°C) of Case 1 and Case 2: (a) exterior wall temperature, $T_{wall,\ s}$ and $T_{wall,\ ns}$; (b) exterior wall temperature difference, $T_{wall,\ diff}$.

is −4.73 °C when snow cover exists, while the average exterior wall temperature is −4.85 °C with no snow cover. During the daytime, the exterior wall temperature of Case 1 is approximately 1 °C greater than that of Case 2 because, due to the higher albedo of snow, more solar radiation is reflected by snow surface during the daytime. The reflected solar radiation is partially absorbed by building facades and thus leads to a temperature increase on the exterior wall during the daytime.

5.5. Outdoor air temperature

Fig. 11 shows the comparison of the outdoor air temperature at 1.2 m between Case 1 and Case 2. The outdoor air temperature difference, $T_{a,\ diff}$, is defined as.

$$T_{a,diff} = T_{a,s} - T_{a,ns} \quad (30)$$

where $T_{a,\,s}$ is the outdoor air temperature at 1.2 m in the presence of snow cover, and $T_{a,\,ns}$ is the outdoor air temperature at 1.2 m when there is no snow cover.

It can be observed in Fig. 11 that, when snow cover exists, the average outdoor air temperature at 1.2 m is −16.34 °C, while the average outdoor air temperature is −16.19 °C with no snow cover. The snow cover decreased the 1.2 m air temperature by 0.15 °C on average and 1.16 °C at the maximum. It can be considered that the increased outgoing shortwave radiation due to the higher albedo of the snow-covered surface mainly accounted for the temperature decrease [65].

5.6. Thermal comfort

The human parameters that were used to calculate SET* are summarized in Table 4. The residential outdoor activity was considered as walking at a speed of 3.2 km/h. The metabolic heat generation and the garment insulation was chosen according to [66,67].

Table 5 shows the summary of the calculated environmental parameters that were used to calculate SET*. It should be noted that the air temperature is the mean value of the whole urban canopy, and the reflected short-wave radiation only considers the data during the daytime. It can be found that, due to the different radiation conditions, there is a difference between the air temperature and the mean radiant temperature (MRT), and the temperature decrease due to the presence of snow cover is amplified on MRT.

Fig. 12 shows the comparison of the outdoor mean SET* between Case 1 and Case 2. The mean outdoor SET* difference, SET^*_{diff}, is defined as.

$$SET^*_{diff} = SET^*_{s} - SET^*_{ns} \quad (31)$$

where SET^*_{s} is outdoor mean SET* in the presence of snow cover, and SET^*_{ns} is the outdoor mean SET* when there is no snow cover.

It can be found that the outdoor mean SET* has an obvious improvement with the removal of snow cover. The average outdoor mean SET* is 17.41 °C in the presence of snow cover, while the average outdoor mean SET* is 17.84 °C when there is no snow cover. The average outdoor mean SET* decreases 0.43 °C in the presence of snow cover, indicating that the existence of snow cover reduces the thermal comfort of people outside in the cold region.

6. Conclusions

A one-dimensional snow model that accounts for heat transfer within snow cover is developed and is implemented into the urban canopy energy balance model, UDC, to study the effects of snow cover on outdoor thermal climate. Several conclusions can be drawn as follows:

(1) Due to the higher albedo of snow, less radiation is absorbed by the snow cover; thus, the snow surface has a lower temperature compared to that of asphalt pavement and soil. On the other hand, the higher reflected solar radiation leads to a temperature increase in building facades during the daytime when snow cover exists.
(2) The average outdoor air temperature at 1.2 m is −16.34 °C in the presence of snow cover, and the average outdoor air temperature is −16.19 °C with no snow cover. The snow cover decreased the 1.2 m air temperature by 0.15 °C on average and 1.16 °C at maximum.
(3) The average outdoor mean SET* in the presence of snow cover is 0.43 °C less than that of the mean SET* when there is no snow cover, indicating that the thermal comfort for people outside has deteriorated due to the existence of snow cover.

Considering the complexity of real snow conditions, several assumptions and simplifications have been made in our simple one-dimensional snow model, e.g., the snow cover is regarded as stable with no snow melting and no refreezing of liquid water

Table 4
Summary of the human parameters that were used to calculate SET*.

Parameters	Value
Height (m)	1.7
Weight (kg)	60
Garment insulation (clo)	2.43
Metabolic heat generation (W/m^2)	116.1

Table 5
Summary of the environmental parameters that were used to calculate SET*.

Parameters		Average	Min	Max
Wind velocity (m/s)	Case 1	0.42	0.07	0.88
	Case 2	0.42	0.09	0.88
Specific humidity (g/kg)	Case 1	0.68	0.22	1.72
	Case 2	0.70	0.24	1.73
Upward long-wave radiation (W/m^2)	Case 1	222.96	208.22	241.26
	Case 2	229.11	218.37	248.38
Reflected short-wave radiation (W/m^2)	Case 1	23.04	0.06	92.49
	Case 2	11.19	0.03	44.91
Air temperature (°C)	Case 1	−16.80	−27.15	−5.30
	Case 2	−16.75	−27.06	−5.28
Mean radiant temperature (°C)	Case 1	−17.91	−25.97	−6.03
	Case 2	−16.05	−22.34	−2.14

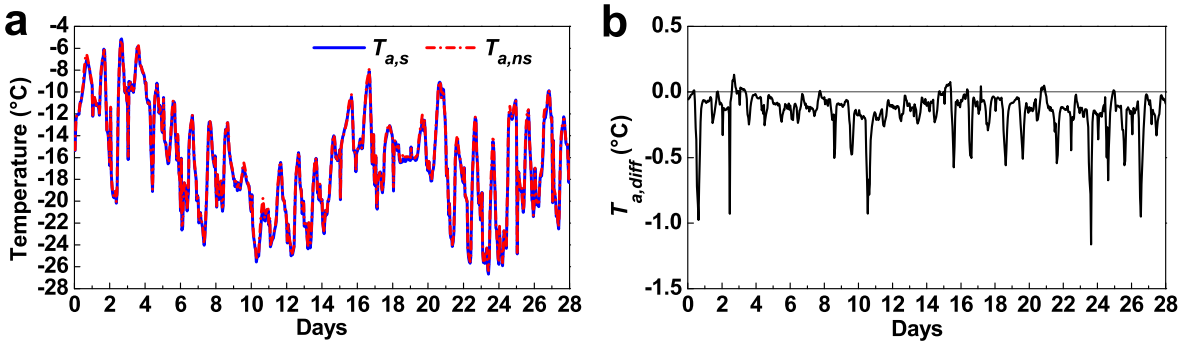

Fig. 11. Comparison of the temperature (°C) at 1.2 m between Case 1 and Case 2: (a) outdoor air temperature, $T_{a,\,s}$ and $T_{a,\,ns}$; (b) outdoor air temperature difference, $T_{a,\,diff}$.

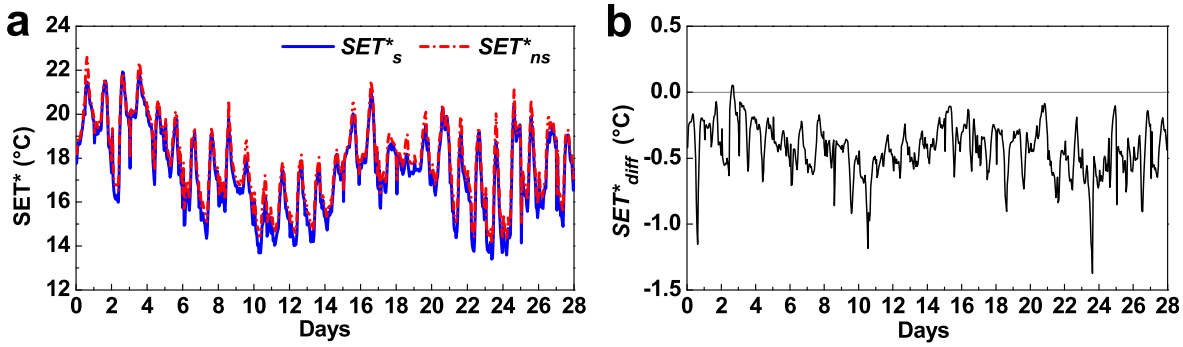

Fig. 12. Comparison of outdoor SET* (°C) between Case 1 and Case 2: (a) mean outdoor SET*, SET^*_s and SET^*_{ns}; (b) mean outdoor SET* difference, SET^*_{diff}.

within the snow cover. In addition, precipitation is also neglected in the snow model. Therefore, a more sophisticated snow model is required to be established in our further work.

Acknowledgments

This research is partially supported by the Fundamental Research for the Central Universities (Grant No. HIT.KISTP.201419) and the NSFC (No. 51438005).

References

[1] CSB (National Bureau of Statistics of China), China statistical Yearbook, Chinese Statistics Press, Beijing, 2012 [in Chinese].
[2] S.J. Wang, C.L. Fang, X.L. Guan, B. Pang, H. Ma, Urbanization, energy consumption, and carbon dioxide emissions in China: a panel data analysis of China's provinces, Appl. Energy 136 (2014) 738–749.
[3] H.H. Feng, X.F. Zhao, F. Chen, L.C. Wu, Using land use change trajectories to quantify the effects of urbanization on urban heat island, Adv. Space Res. 53 (2014) 463–473.
[4] L.L. Cui, J. Shi, Urbanization and its environmental effects in Shanghai, China, Urban Clim. 2 (2012) 1–15.
[5] L.J. Han, W.Q. Zhou, W.F. Li, L. Li, Impact of urbanization level on urban air quality: a case of fine particles (PM2.5) in Chinese cities, Environ. Pollut. 194 (2014) 163–170.
[6] A.M. Rizwan, L.Y.C. Dennis, C. Liu, A review on the generation, determination and mitigation of urban heat island, J. Environ. Sci. 20 (1) (2008) 120–128.
[7] F. Busato, R.M. Lazzarin, M. Noro, Three years of study of the Urban Heat Island in Padua: experimental results, Sustain. Cities Soc. 10 (2014) 251–258.
[8] B. Chun, J.M. Guldmann, Spatial statistical analysis and simulation of the urban heat island in high-density central cities, Landsc. Urban Plan. 125 (2014) 76–88.
[9] P. Pandey, D. Kumar, A. Prakash, et al., A study of urban heat island and its association with particulate matter during winter months over Delhi, Sci. Total Environ. 414 (5) (2012) 494–507.
[10] Y.Y. Li, H. Zhang, W. Kainz, Monitoring patterns of urban heat islands of the fast-growing Shanghai metropolis, China: using time-series of Landsat TM/ETM+ data, Int. J. Appl. Earth Observat. Geoinformat. 19 (2012) 127–138.
[11] M. Kolokotroni, R. Giridharan, Urban heat island intensity in London: an investigation of the impact of physical characteristics on changes in outdoor air temperature during summer, Sol. Energy 82 (2008) 986–998.
[12] M.A. Lokoshchenko, Urban 'heat island' in Moscow, Urban Clim. 10 (2014) 550–562.
[13] A.L. Pisello, F. Rossi, F. Cotana, Summer and winter effect of innovative cool roof tiles on the dynamic thermal behavior of buildings, Energies 7 (2014) 2343–2361.
[14] F. Cotana, F. Rossi, M. Filipponi, et al., Albedo control as an effective strategy to tackle Global Warming: a case study, Appl. Energy 130 (2014) 641–647.
[15] F. Rossi, B. Castellani, A. Presciutti, et al., Retroreflective façades for urban heat island mitigation: experimental investigation and energy evaluations, Appl. Energy 145 (2015) 8–20.
[16] A.G. Touchaei, H. Akbari, The climate effects of increasing the albedo of roofs in a cold region, Adv. Build. Energy Res. 7 (2) (2013) 186–191.
[17] T. Karlessi, M. Santamouris, K. Apostolakis, et al., Development and testing of thermochromic coatings for buildings and urban structures, Sol. Energy 83 (2009) 538–551.
[18] P.A. Mirzaei, F. Haghighat, Approaches to stydy Urban Heat Island – abilities and limitations, Build. Environ. 45 (2010) 2192–2201.
[19] E.G. McPherson, L.P. Herrington, G.M. Heisler, Impacts of vegetation on residential heating and cooling, Energy Build. 12 (1) (1988) 41–51.
[20] R. Giridharan, M. Kolokotroni, Urban heat island characteristics in London during winter, Sol. Energy 83 (1) (2009) 1668–1682.
[21] L. Yang, H.Y. Yan, Y. Xu, et al., Residential thermal environment in cold climates at high altitudes and building energy use implications, Energy Build. 62 (2013) 139–145.
[22] S. Dhaka, J. Mathur, G. Brager, et al., Assessment of thermal environmental conditions and quantification of thermal adaptation in naturally ventilated buildings in composite climate of India, Build. Environ. 86 (2015) 17–28.
[23] S.Q. Gou, Z.G. Li, Q. Zhao, et al., Climate responsive strategies of traditional dwellings located in an ancient village in hot summer and cold winter region of China, Build. Environ. 86 (2015) 151–165.
[24] M.J. Zhao, J. Srebric, Assessment of Green Roof Performance for Sustainable Buildings under Winter Weather Conditions, vol. 19, Journal of Central South University of Technology, 2012, pp. 639–644.
[25] M. Taleghani, M. Tenpierik, A. van den Dobbelsteen, et al., Heat mitigation strategies in winter and summer: Field measurements in temperate climates, Build. Environ. 81 (2014) 309–319.
[26] J.E. Walsh, D.R. Tucek, M.R. Peterson, Seasonal snow cover and short-term climatic fluctuations over the United States, Mon. Weather Rev. 110 (1982) 1474–1486.
[27] T.L. Mote, On the Role of Snow Cover in Depressing Air Temperature, J. Appl. Meteorol. Climatol. 47 (2008) 2008–2022.
[28] J.H.M. Beyers, P.A. Sundsbo, T.M. Harms, Numerical simulation of three-dimensional transient snow drifting around a cube, J. Wind Eng. Ind. Aerodynamics 92 (2004) 725–747.
[29] J.H.M. Beyers, W.F. Waechter, H.A. Baker, et al., Modelling transient snowdrift development around complex three-dimensional structures, in: The Fourth International Symposium on Computational Engineering, 2006. Yokohama, Japan.
[30] Y. Tominaga, T. Okaze, A. Mochida, et al., Prediction of snowdrift around a cube using CFD Model incorporating effect of snow particles on turbulent flow, in: The Seventh Asia-Pacific Conference on Wind Engineering, 2009. Taipei, Taiwan.
[31] Y. Tominaga, T. Okaze, A. Mochida, et al., Basic investigation of modeling for erosion and accumulation on snow surface, J. Environ. ENG. AIJ 74 (643) (2009) 1083–1089.
[32] Y. Tominaga, Numerical prediction of snow drift around buildings using CFD, J. Snow Eng. Jpn. 26 (4) (2010) 80–89.
[33] S. Bélair, J. Mailhot, A. Lemonsu, et al., The Montréal Urban Snow Experiments (MUSE), Int. Assoc. Urban Clim. (IAUC) Newsl. 16 (2006) 9–10.
[34] A. Lemonsu, S. Bélair, J. Mailhot, et al., Overview and first results of the Montreal Urban Snow Experiment 2005, J. Appl. Meteorology Climatol. (2008) 59–75.
[35] O. Bergeron, I.B. Strachan, Wintertime radiation and energy budget along an urbanization gradient in Montreal, Canada, Int. J. Climatol. 32 (1) (2012) 137–152.
[36] A. Lemonsu, S. Bélair, J. Mailhot, et al., Evaluation of the town energy balance model in cold and snowy conditions during the Montreal Urban Snow Experiment 2005, J. Appl. Meteorology Climatol. 49 (3) (2010) 346–362.
[37] S. Leroyer, J. Mailhot, S. Bélair, et al., Modeling the surface energy budget during the thawing period of the 2006 Montreal Urban Snow Experiment, J. Appl. Meteorology Climatol. 49 (2010) 68–84.
[38] V.A. Masson, Physically-Based Scheme for the Urban Energy Budget in Atmospheric Models, Boundary-Layer Meteorol. 94 (2000) 357–397.
[39] C.S.B. Grimmond, M. Blackett, M. Best, et al., The international urban energy balance models comparison project: first results from phase 1, J. Appl. Meteorology Climatol. 49 (6) (2010) 1268–1292.
[40] C.S.B. Grimmond, M. Blackett, M. Best, et al., Initial results from phase 2 of the international urban energy balance model comparison, Int. J. Climatol. 31 (2011) 244–272.
[41] W.S. Wei, D.H. Qin, M.Z. Liu, Properties and structure of the seasonal snow cover in the northwest regions of China, Arid. land Geogr. 24 (4) (2001) 310–313 [in Chinese with English abstract].
[42] E.A. Anderson, A point energy and mass balance model of a snow cover, NOAA

Tech. Rep. NWS 19 (1976) 150.
[43] Snow Hydrology. Summary reports of the snow investigations. Portland, Oregan: North Pacific Division, Corps of Engineers, U.S. Army: 437.
[44] A. Fujimoto, H. Watanabe, T. Fukuhara, Thermal contact resistance between the pavement surface and snow layer, Jpn. Soc. Civ. Eng. Proc. 63 (2007) 156–165 [in Japanese with English abstract].
[45] 2009 ASHRAE Handbook: Fundamentals – IP Edition, American Society of Heating, Refrigerating and Air-Conditioning Engineers, Atlanta, 2009.
[46] J. Kondo, H. Yamazawa, Bulk transfer coefficient over a snow surface, Bound. Layer. Meteorol. 34 (1986) 123–135.
[47] Y.M. Zhu, J. Liu, A. Hagishima, J. Tanimoto, J. Yao, Z.L. Ma, Evaluation of coupled outdoor and indoor thermal comfort environment and anthropogenic heat, Build. Environ. 42 (2007) 1018–1025.
[48] Y.M. Zhu, J. Liu, Y. Yao, et al., Evaluating the impact of solar radiation on outdoor thermal comfort by the development and validation of a simple urban climatic model, in: International Solar Energy Conference, July 8–13, 2006. Denver, USA.
[49] J.Q. Rao, J. Liu, R.B. Xiao, H.Y. Liang, Field Measurement and Simulation of the Micro-thermal Climate in a Typical Dwelling District in China: the Guangzhou Case, IWEERB2014, Zhengzhou, China, Nov.8–10, 2014.
[50] H. Kondo, F. Liu, A study on the urban thermal environment obtained through one-dimensional urban canopy model, J. Jpn Soc Atmos Environ 33 (3) (1998) 179–192 [in Japanese with English abstract].
[51] J.T. Shao, J. Liu, J.N. Zhao, W.W. Zhang, D.X. Sun, Z.P. Fu, A novel method for full-scale measurement of the external convective heat transfer coefficient for building horizontal roof, Energy Build. 41 (8) (2009) 840–847.
[52] T. Koji, K. Tadahisa, T. Jun, et al., A proposal of evaporation raito dumping model for artificial covering watted with precipitation: part3 model improvement, in: Summaries of Technical Papers of Annual Meeting, 2000, pp. 351–352. D-2, [in Japanese with English abstract].
[53] H. Aya, T. Jun, K. Tadahisa, et al., Parameter identification of simplified model of soil evaporation with numerical experiments using the hygrothermal dynamics model: a study on simplified estimation of evaporation rate from soil surface Part 2, J. Archit Plann Environ Eng AIJ 540 (2001) 67–72 [in Japanese with English abstract].
[54] K. Harumi, K. Tadahisa, H. Tetsuo, et al., E Experimental study on effect of lawn surface on thermal environmento in ruban aera: hygrothermal charactreistics of lawn surface Part 2, J. Archit Plann Environ Eng AIJ 507 (5) (1998) 7–12 [in Japanese with English abstract].
[55] Z. Sang, H. Liu, H. Liu, Z. Zhang, Observational and numerical studies of wintertime urban boundary layer, J. Wind Eng. Industrial Aerodynamics 87 (2000) 243–258 [in Chinese with English abstract].
[56] P. Höppe, Different aspects of assessing indoor and outdoor thermal comfort, Energy Build. 34 (6) (2002) 661–665.
[57] A.P. Gagge, A. Fobelets, L.G. Berglund, A standard predictive index of human response to the thermal environment, ASHRAE Trans. 92 (1986) 709–731.
[58] A. Ishii, T. Katayama, Y. Shiotsuki, et al., Experimental study on comfort perception of people in the outdoor environment. Journal of architecture, planning and environmental engineering, Trans. AIJ 386 (1988) 28–37 [in Japanese with English abstract].
[59] S. Jennifer, D. Richard, A field study of thermal comfort in outdoor and semi-outdoor environments in subtropical Sydney Australia, Build. Environ. 38 (5) (2003) 721–738.
[60] T. Kinouchi, A study on thermal indices for the outdoor environment, Tenki 48 (2001) 661–671 [in Japanese with English abstract].
[61] T. Honjo, Thermal Comfort in Outdoor Environment, Glob. Environ. Res. 13 (2009) 43–47.
[62] DB23/1270—2008. Design Standard for Energy Efficiency of Residential Buildings in Heilongjiang Province.
[63] Q.Y. Zhang, H.X. Yang, Typical Meteorological Database Handbook for Buildings, China Building Industry Press, Beijing, 2012 [in Chinese].
[64] Q.Y. Zhang, Development of the typical meteorological database for Chinese locations, Energy Build. 38 (2006) 1320–1326.
[65] D.G. Baker, D.L. Ruschy, R.H. Skaggs, D.B. Wall, Air temperature and radiation depressions associated with a snow cover, J. Appl. Meteorology Climatol. 31 (1992) 247–254.
[66] ASHRAE. American Society of Heating, Refrigerating and Air Conditioning Engineers Handbook 2001 Fundamentals, Chap. 8. Thermal Comfort, 8.1–8.28.
[67] Y. Jiang, Y.X. Zhu, R.H. Skaggs, D.B. Wall, Design temperature of underground stations in winter, HV&AC 32 (4) (2002) 20–22 [in Chinese with English abstract].